

Supporting information for

**Precise peripheral design enables propeller-like squaraine dye with highly sensitive and wide-range piezochromism**

Weihan Guo <sup>a</sup>, Mingda Wang <sup>a</sup>, Leilei Si <sup>a</sup>, Yigang Wang <sup>a</sup>, Guomin Xia <sup>a, \*</sup>, Hongming Wang <sup>a, b</sup>

<sup>a</sup> Institute for Advanced Study, Nanchang University, Nanchang 330031, China.

Email: guominxia@ncu.edu.cn

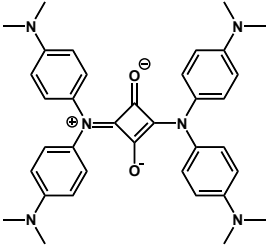
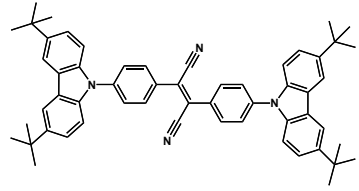
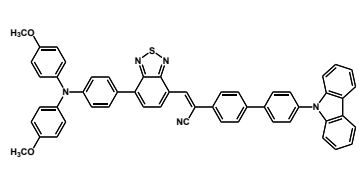
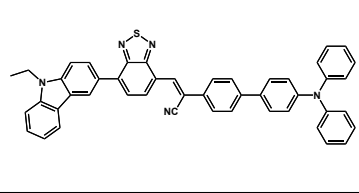
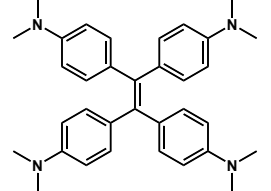
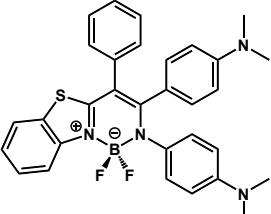
<sup>b</sup> College of Chemistry and Chemical Engineering, Nanchang University, Nanchang 330031, China.

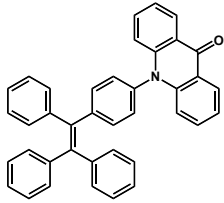
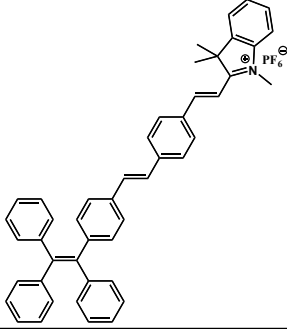
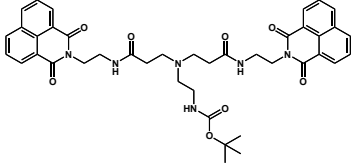
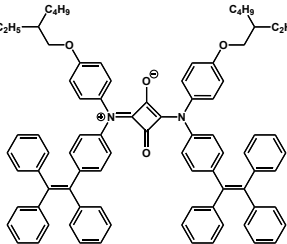
**Table of Contents**

The photophysical data and pressure required for the reported PCF materials .....	2
Materials and Methods .....	3
Synthesis of SQs .....	4
Photophysical properties of SQ-NMe <sub>2</sub> in solution.....	6
Preparations and characterizations of all crystalline assemblies.....	7
Photophysical properties of SQ-NMe <sub>2</sub> in crystal .....	7
Crystal data and characterizations of SQ-NMe <sub>2</sub> microcrystals.....	9
Crystal data and crystal structure analyses of SQ-H and SQ-OMe .....	14
Characterizations and all photophysical data of SQ-H and SQ-OMe microcrystals ...	18
Computational study .....	21
Details of cryptographic application .....	23
<sup>1</sup> H NMR, <sup>13</sup> C NMR and MS spectra .....	24
References .....	28

## The photophysical data and pressure required for the reported PCF materials

**Table S1** The photophysical data and pressure required for the reported PCF materials.

Structure	Emission				Pressure required	References
	Before grinding		After grinding			
	$\lambda_{em}$ [nm]	$\Phi_{PL}$ %	$\lambda_{em}$ [nm]	$\Phi_{PL}$ %		
	554	36.9	648	23.7	Hand-actuated grinding	Our work
	538	58	588	53	0.5 MPa	Adv. Funct. Mater., 2020, 30, 2000105.
	615	60.7	775	5.2	Machine-actuated grinding	Angew. Chem. Int. Ed. 2021, 60, 8510-8514.
	586	47	646	34	0.6 MPa	Adv. Optical Mater. 2021, 9, 2100598.
	460	98	497	67	Hand-actuated grinding	J. Phys. Chem. C 2013, 117, 24997-25003.
	518	27	582	\	< 1.5 GPa	Chem. Commun., 2015, 51, 7497-7500.

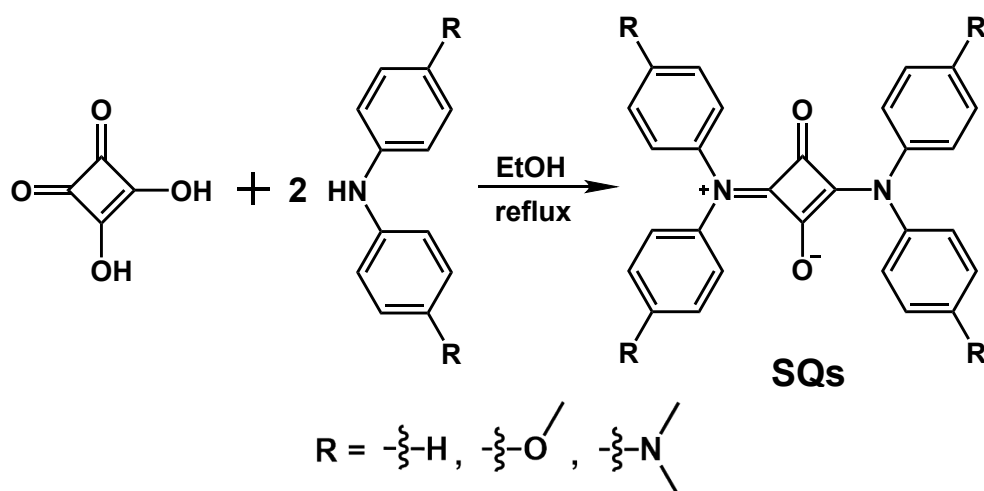
	423	1	520	43	2.98 GPa	Adv. Funct. Mater. 2015, 25, 4005-4010.
	638	10.19	707	3.71	Hand-actuated grinding	J. Mater. Chem. C, 2015, 3, 12328.
	410	9.8	464	2.6	Hand-actuated grinding	Small, 2018, 14, 1802524.
	534	13	602	8.8	Hand-actuated grinding	Mater. Chem. Front., 2020, 4, 2688-2696.

## Materials and Methods

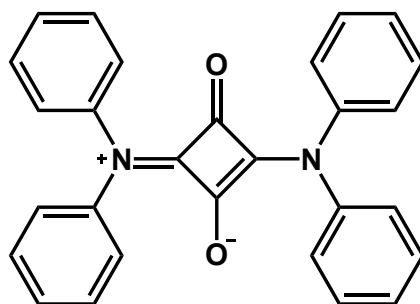
All chemicals and solvents were purchased from commercial suppliers and used as received unless explicitly stated.  $^1\text{H}$  NMR and  $^{13}\text{C}$  NMR spectra were measured on a Bruker AVANCE III HD 400MHz spectrometer (Bruker, Germany) in  $\text{DMSO-}d_6$  or  $\text{DCM-}d_2$  using tetramethylsilane (TMS) as an internal standard. High-resolution mass spectra (HRMS) were recorded using a UHPLC30A-Trip TOF 5600<sup>+</sup> (SCIEX, Japan). The UV-vis absorption spectra in the solution were recorded on a Lambda 750 spectrophotometer (PerkinElmer, USA). The UV-vis absorption spectra in the crystal were recorded on a UV-3600 spectrophotometer (Shimadzu, Japan). The photoluminescence (PL) spectra were recorded on a FluoroMax-4 luminescence spectrometer (Horiba, France). The absolute PL quantum efficiencies ( $\Phi_{\text{PL}}$ ) were

determined using a Horiba FL-3018 Integrating Sphere. The fluorescence lifetime measurement was performed on a Horiba FluoreCube spectrofluorometer system using a UV diode laser for excitation. Thermogravimetric analysis (TGA) was carried out on a TG/DTA instrument (PerkinElmer STA 6000, USA) at a heating rate of 20 °C min<sup>-1</sup> under an N<sub>2</sub> atmosphere. Powder X-ray diffraction (PXRD) data were collected using an XD-2 Purkinje multicrystal X-ray diffractometer. The differential scanning calorimetry (DSC) curves were performed on a TA instrument (America, DSC2500).

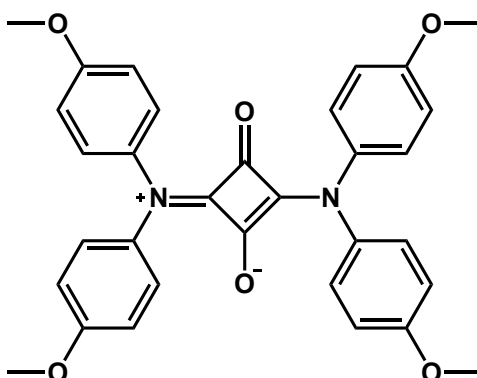
### Synthesis of SQs



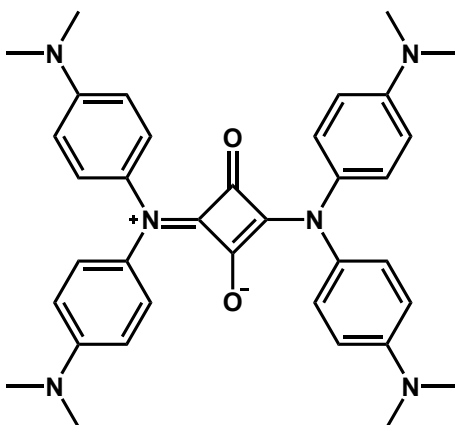
To a 50 mL round bottom flask was added squaric acid (228 mg, 2 mmol) and corresponding diphenylamines (2.2 equiv) in 25 mL distilled ethanol (EtOH). After stirring for 3 h at 80 °C, the mixture was cooled to room temperature and filtered, and the obtained solid residue was washed with EtOH to afford corresponding SQs. Further purification was performed by recrystallization from N, N-dimethylformamide (DMF), and methanol (MeOH) if necessary.



**SQ-H** Diphenylamine (744 mg, 4.4 mmol, 2.2 eq), 80 °C; yellow powder (489 mg, 65.7% yield). <sup>1</sup>H NMR (400 MHz, DMSO-*d*<sub>6</sub>) δ: 7.43 (t, J = 8.0 Hz, 8H; Ar H), 7.34 (t, J = 8.0 Hz, 4H; Ar H), 7.24 (d, J = 8.0 Hz, 8H; Ar H) ppm; <sup>13</sup>C NMR (100 MHz, DCM-*d*<sub>2</sub>) δ: 211.75, 163.51, 139.62, 128.00, 126.75, 124.64 ppm; HRMS (ESI) m/z: [M + H]<sup>+</sup> calcd, 417.1525; found, 417.1587.



**SQ-OMe** 4,4'-Dimethoxydiphenylamine (1.01 g, 4.4 mmol, 2.2 eq), 80 °C; orange powder (759 mg, 75.1% yield). <sup>1</sup>H NMR (400 MHz, DMSO-*d*<sub>6</sub>) δ: 7.135 (d, J = 12.0 Hz, 8H; Ar H), 6.95 (d, J = 8.0 Hz, 8H; Ar H), 3.78 (s, 12H; CH<sub>3</sub>) ppm; <sup>13</sup>C NMR (100 MHz, DCM-*d*<sub>2</sub>) δ: 157.96, 133.13, 125.56, 113.02, 54.74 ppm (two carbon signals were not detected due to poor solubility); HRMS (ESI) m/z: [M + H]<sup>+</sup> calcd, 537.1947; found, 537.2012.



**SQ-NMe<sub>2</sub>** Bis(4-dimethylaminophenyl) amine (1.12 g, 4.4 mmol, 2.2 eq), 80 °C; orange powder (643 mg, 57.4% yield). <sup>1</sup>H NMR (400 MHz, DMSO-*d*<sub>6</sub>) δ: 6.97 (d, J = 8.0 Hz, 8H; Ar H), 6.69 (d, J = 8.0 Hz, 8H; Ar H), 2.92 (s, 24H; CH<sub>3</sub>) ppm; <sup>13</sup>C NMR (100 MHz, DCM-*d*<sub>2</sub>) δ: 168.40, 148.59, 129.88, 124.99, 110.86, 39.57 ppm (one carbon

signal were not detected due to poor solubility); HRMS (ESI)  $m/z$ :  $[M + H]^+$  calcd, 589.3213; found, 589.3279.

### Photophysical properties of SQ-NMe<sub>2</sub> in solution

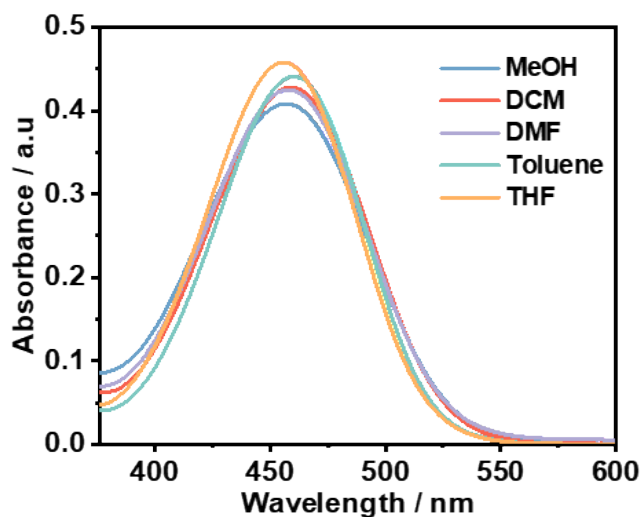


**Fig. S1** Absorption spectra of SQ-NMe<sub>2</sub> (50 μM) in different solvents.

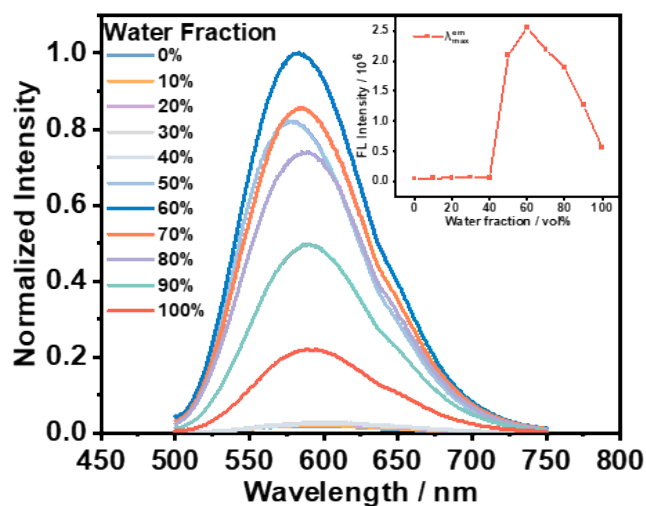


**Fig. S2** PL spectra of SQ-NMe<sub>2</sub> (50 μM) in DMF solution with different fractions of water. (Inset: Plots of  $\lambda_{em}$  max with different fractions of water, where  $\lambda_{em}$  max depicts the maximum emission intensity)

## Preparations and characterizations of all crystalline assemblies

**Single-Crystal X-Ray Crystallography:** The single crystals of SQ-H, SQ-OMe, and SQ-NMe<sub>2</sub> Y-form can be easily obtained by recrystallization in DMF and MeOH solution. Meanwhile, the SQ-NMe<sub>2</sub> O-form was obtained by the slow evaporation in dichloromethane (DCM). All the X-ray diffraction experiments were carried out on a Japan Rigaku XtaLAB Synergy Custom Single-crystal diffractometer at 100K or 200K. The structures were resolved and analyzed with the assistance of Olex2 software.

**Preparation of Microcrystals:** The needle-like SQ-H and SQ-OMe crystals were prepared via a liquid phase self-assembly method. 50 mg SQ-H or SQ-OMe was wholly dissolved in the 5 mL refluxing DMF solution with vigorous sonication for 20 min. Meanwhile, the SQ-NMe<sub>2</sub> microcrystals can be prepared via recrystallization in DMF and MeOH solution (Y-form) or slow evaporation in DCM (O-form). After cooling and aging in closed tubes at room temperature for 30 min, the corresponding assemblies with uniform dimensions were formed in the solution. These microcrystals were then filtrated, and the obtained SQs assemblies were exposed at room temperature for 1 h for further characterization.

## Photophysical properties of SQ-NMe<sub>2</sub> in crystal

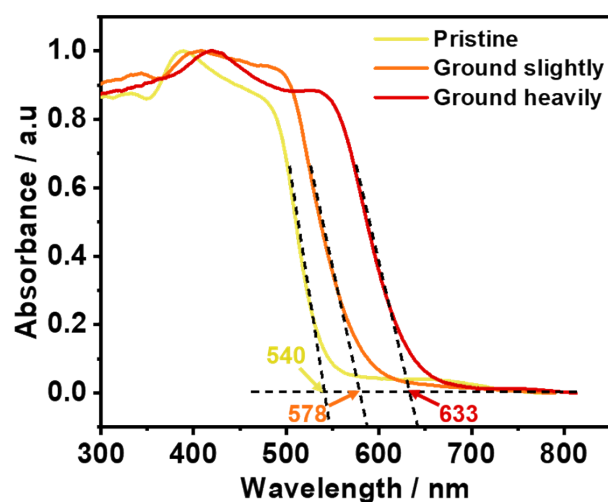


**Fig. S3** Absorption spectra of SQ-NMe<sub>2</sub> (Pristine, Ground slightly and Ground heavily) in crystal.

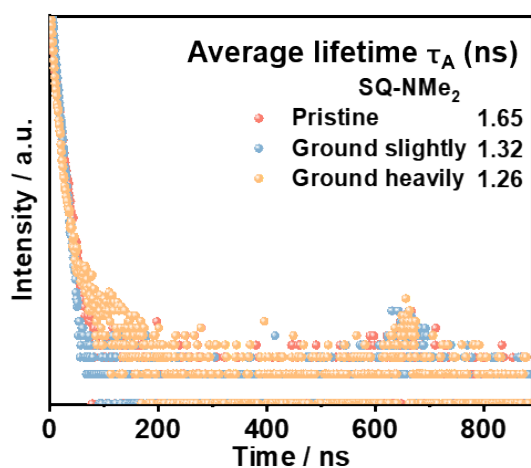


**Fig. S4** Lifetime decay profiles of SQ-NMe<sub>2</sub> (Pristine, Ground slightly and Ground heavily) in crystal.

**Table S2** The photophysical data for pristine and treated SQ-NMe<sub>2</sub> microcrystals.

State	$\lambda_{em}$ <sup>a)</sup> [nm]	$\Phi_{PL}$ <sup>b)</sup> %	Lifetime $\tau_f$ <sup>c)</sup> [ns]	$\chi^2$	$k_f$ <sup>d)</sup> [10 <sup>7</sup> s <sup>-1</sup> ]	$k_{nr}$ <sup>e)</sup> [10 <sup>7</sup> s <sup>-1</sup> ]
Pristine	554	36.9	1.65	1.05	22.36	38.24
Ground slightly	590	31.5	1.32	1.04	23.86	51.89
Ground heavily	648	23.7	1.26	1.07	18.81	60.56

<sup>a)</sup> Measured using an integrating sphere method; <sup>b)</sup> Measured using a single-photocounting method; <sup>c)</sup> Radiative rate constant ( $k_f = \Phi_{PL} / \tau_f$ ); <sup>d)</sup> Nonradiative rate constant ( $k_{nr} = (1 - \Phi_{PL}) / \tau_f$ ).

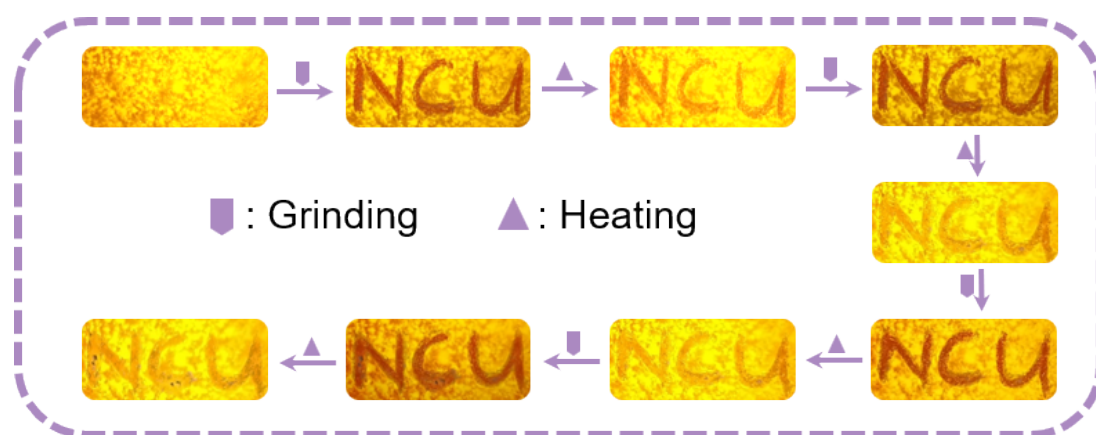


**Fig. S5** The reversible fluorescence photographs of SQ-NMe<sub>2</sub> microcrystals at two conditions (grinding and heating) for 5 cycles.



## Crystal data and characterizations of SQ-NMe<sub>2</sub> microcrystals

**Table S3** Crystallographic data of SQ-NMe<sub>2</sub> Y-form, SQ-NMe<sub>2</sub> O-form.

Sample	SQ-NMe <sub>2</sub> Y-form	SQ-NMe <sub>2</sub> O-form
CCDC number	2248407	2248408
Empirical formula	C <sub>36</sub> H <sub>40</sub> N <sub>6</sub> O <sub>2</sub>	8(C <sub>36</sub> H <sub>40</sub> N <sub>6</sub> O <sub>2</sub> )11(CH <sub>2</sub> Cl <sub>2</sub> )
Formula weight	588.74	5644.09
<i>T</i> [K]	200.0	200.00(10)
Crystal system	monoclinic	orthorhombic
Space group	C 1 2/c 1	P b c a
<i>a</i> [Å]	22.5871(9)	8.5815(2)
<i>b</i> [Å]	6.0324(2)	23.7567(5)
<i>c</i> [Å]	25.2819(10)	38.1133(12)
$\alpha$ [°]	90	90
$\beta$ [°]	114.529(5)	90
<i>Z</i>	90	90
<i>V</i> [Å <sup>3</sup> ]	3133.9(2)	7770.1(3)
<i>Z</i>	4	1
F (000)	1256	2974
density [g/cm <sup>3</sup> ]	1.248	1.206
$\mu$ [mm <sup>-1</sup> ]	0.627	0.080
Reflections collected	9535	39616
unique reflections	3258	7677
<i>R</i> (int)	0.019	0.053
GOF	1.054	1.130
<i>R</i> <sub>1</sub> [ <i>I</i> > 2σ( <i>I</i> )]	0.046	0.092
$\omega R_2$ [ <i>I</i> > 2σ( <i>I</i> )]	0.122	0.239
<i>R</i> <sub>1</sub> (all data)	0.056	0.122
$\omega R_2$ (all data)	0.128	0.259

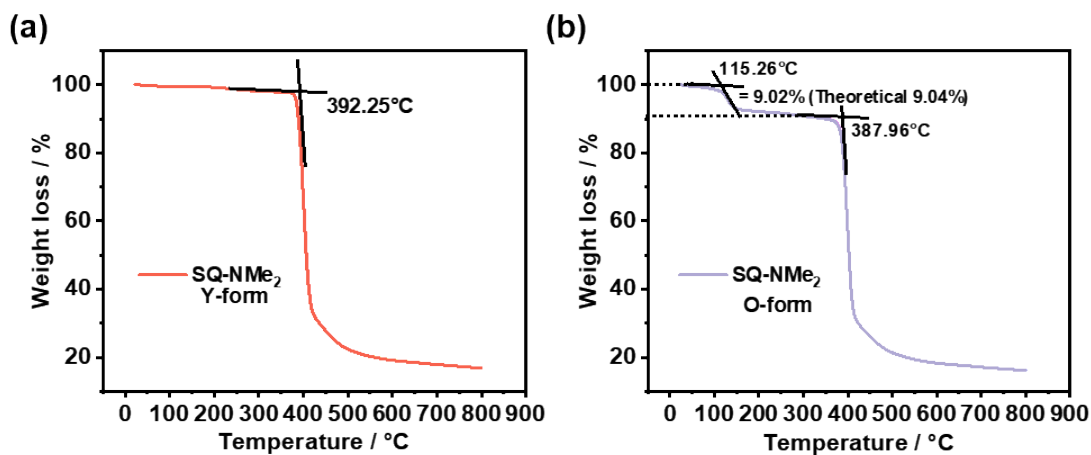


**Fig. S6** TGA curves of (a) SQ-NMe<sub>2</sub> Y-form, (b) SQ-NMe<sub>2</sub> O-form microcrystals. The scanning rate is 20 °C min<sup>-1</sup> under N<sub>2</sub>.

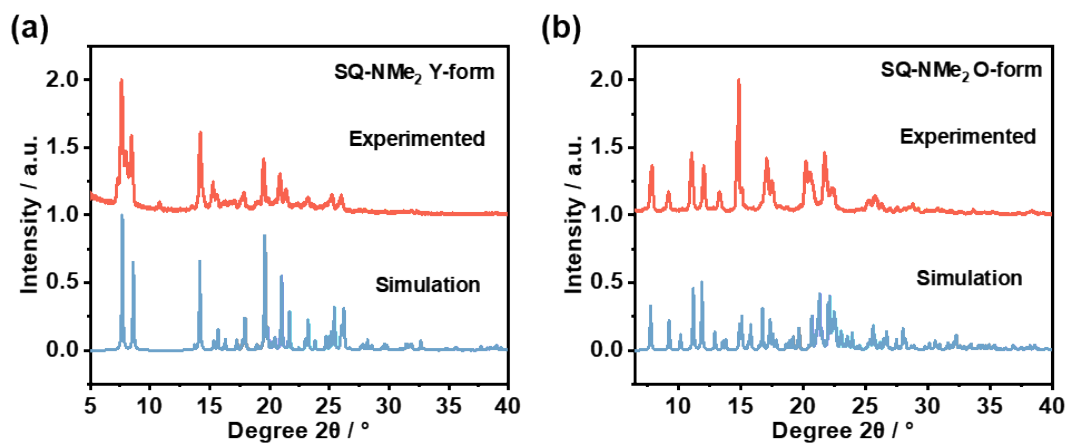


**Fig. S7** PXRD patterns of (a) SQ-NMe<sub>2</sub> Y-form, (b) SQ-NMe<sub>2</sub> O-form: simulated and experimented sample.

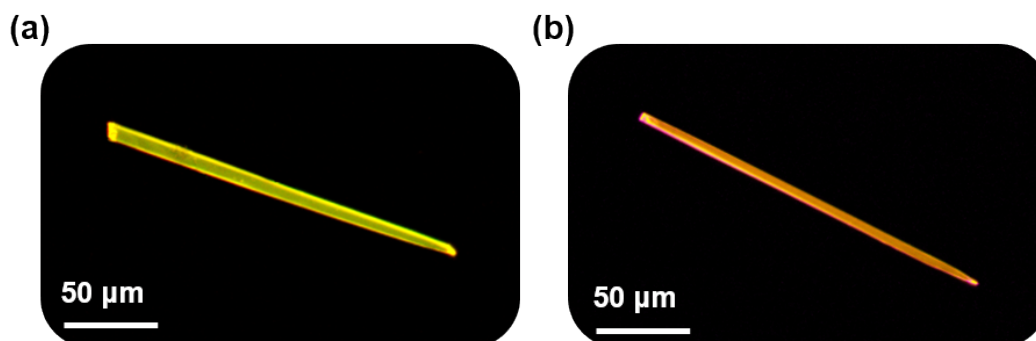


**Fig. S8** Fluorescence microscope images (under 365 nm UV illumination) of (a) SQ-NMe<sub>2</sub> Y-form, (b) SQ-NMe<sub>2</sub> O-form crystals.

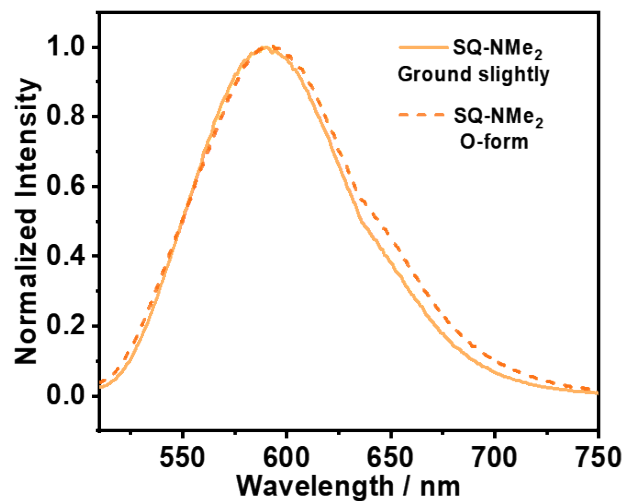


**Fig. S9** Normalized PL spectra of SQ-NMe<sub>2</sub> (Ground slightly) and SQ-NMe<sub>2</sub> O-form in crystal.

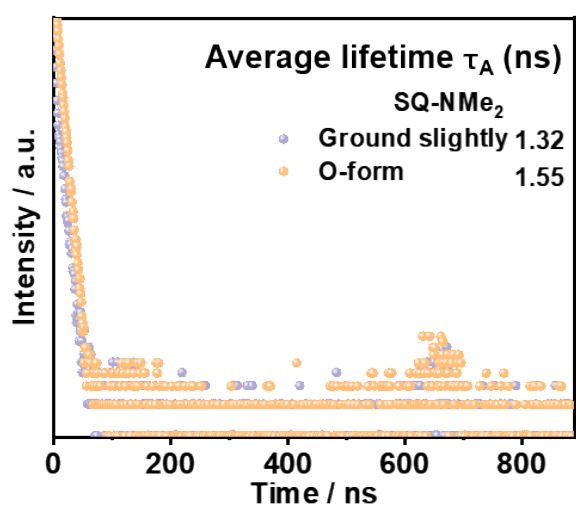


**Fig. S10** Lifetime decay profiles of SQ-NMe<sub>2</sub> (Ground slightly) and SQ-NMe<sub>2</sub> O-form in crystal.

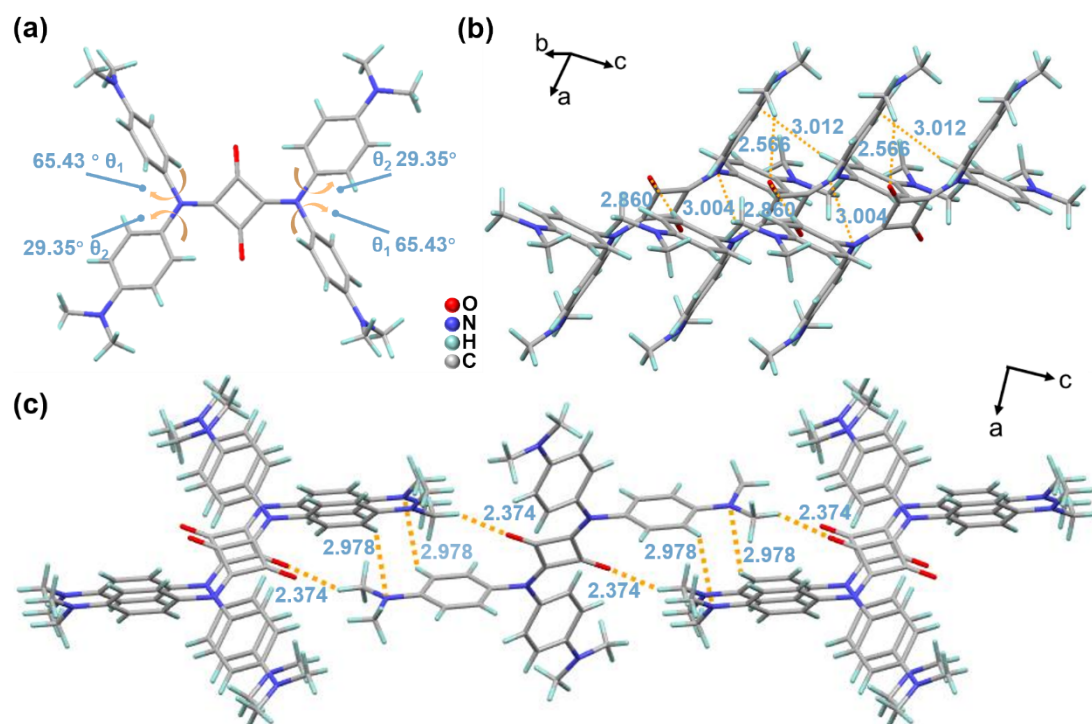


**Fig. S11** The molecular structure and packing mode in the SQ-NMe<sub>2</sub> Y-form crystal. (a) The torsion angles between the four-membered ring and phenyl rotors in front view. Multiple intermolecular hydrogen bonding interactions between adjacent SQ-NMe<sub>2</sub> molecules along (b) a, b-axis and (c) a, c-axis.

SQ-NMe<sub>2</sub> Y-form crystal belonged to a monoclinic crystal system and crystallized in the space group of C 2/c with four SQ-NMe<sub>2</sub> molecules in one unit cell, taking the parameters of  $a = 22.5871(9)$ ,  $b = 6.0324(2)$  and  $c = 25.2819(10)$  Å. The torsion angles between the four-membered ring and phenyl moieties were detected as  $\theta_1 = 29.35^\circ$  and  $\theta_2 = 65.43^\circ$  in SQ-NMe<sub>2</sub> (Fig. S11a). Along the a and b axis, there exist multiple intermolecular hydrogen bonding interactions, including Ar-H...O (2.860 Å), Ar-H... $\pi$  (3.012 Å), and Ar-H...N (3.004 Å), thus locking the phenyl rotations. Other types of C-H...O hydrogen bonding interaction (2.566 Å and 2.374 Å) between adjacent SQ-NMe<sub>2</sub> molecules can also be found (Fig. S11b-c). Meanwhile, a weak Ar-H...N hydrogen bonding interaction (2.978 Å) between Ar-H and N, N-dimethyl in the diphenylamine moieties was also observed along the a and c axis. All those hydrogen bonding interactions are soft and well responded to the highly sensitive PCF behavior of SQ-NMe<sub>2</sub> Y-form crystal.

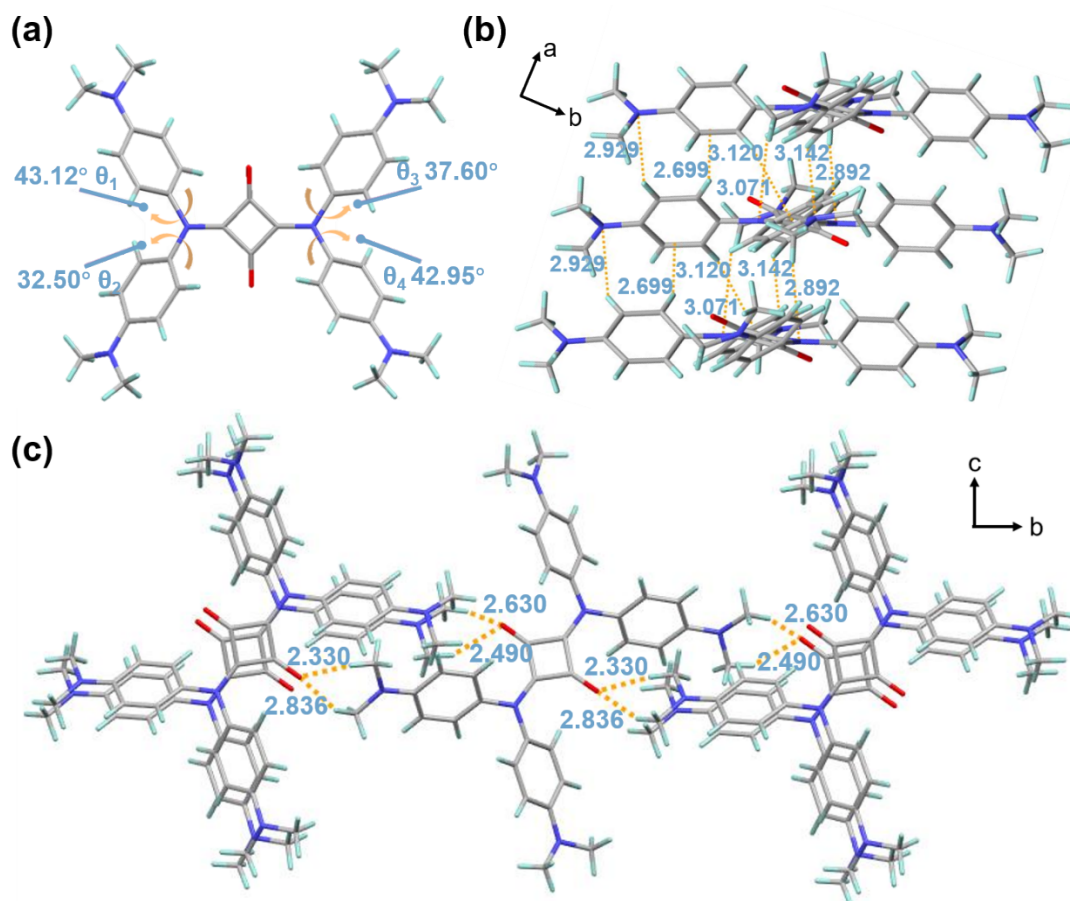


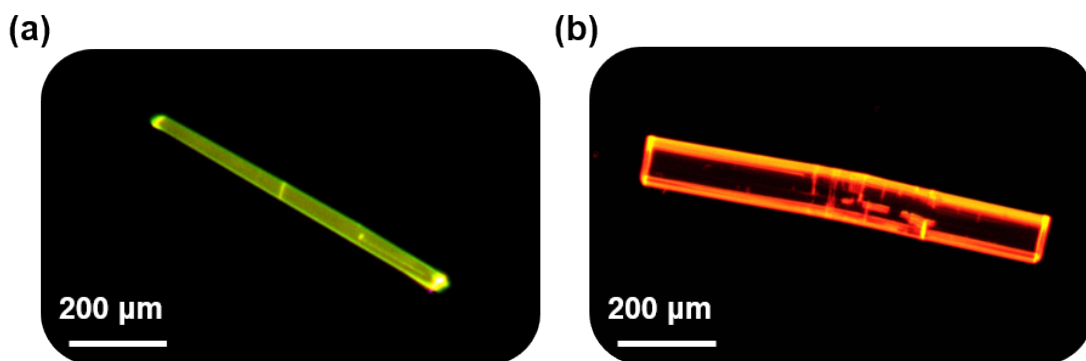
**Fig. S12** The molecular structure and packing mode in the SQ-NMe<sub>2</sub> O-form crystal. (a) The torsion angles between the four-membered ring and phenyl rotors in front view. Multiple intermolecular hydrogen-bonding interactions between adjacent SQ-NMe<sub>2</sub> molecules along (b) a, b-axis and (c) b, c-axis.

SQ-NMe<sub>2</sub> O-form crystal belonged to a monoclinic crystal system and crystallized in the space group of *Pbc* with eight SQ-NMe<sub>2</sub> molecules in one unit cell, taking the parameters of  $a = 8.5815(2)$ ,  $b = 23.7567(5)$  and  $c = 38.1133(12)$  Å. The torsion angles between the four-membered ring and phenyl moieties were detected as 32.50° to 43.12° approximately, which is more planar than SQ-NMe<sub>2</sub> Y-form (Fig. S12a). There are multiple hydrogen bonding interactions, such as Ar-H... $\pi$ , C-H...O, Ar-H...N and Ar-H...O, were observed with the distance range from 2.330 to 3.142 Å between adjacent SQ-NMe<sub>2</sub> molecules (Fig. S12b-c). The interactions exerted on Ar-H contribute largely to locking the phenyl rotations, which are richer than SQ-NMe<sub>2</sub> O-form but still soft, thus accounting for the deep red emission of orange SQ-NMe<sub>2</sub> microcrystals arising from further conformational planarization under heavy grinding.

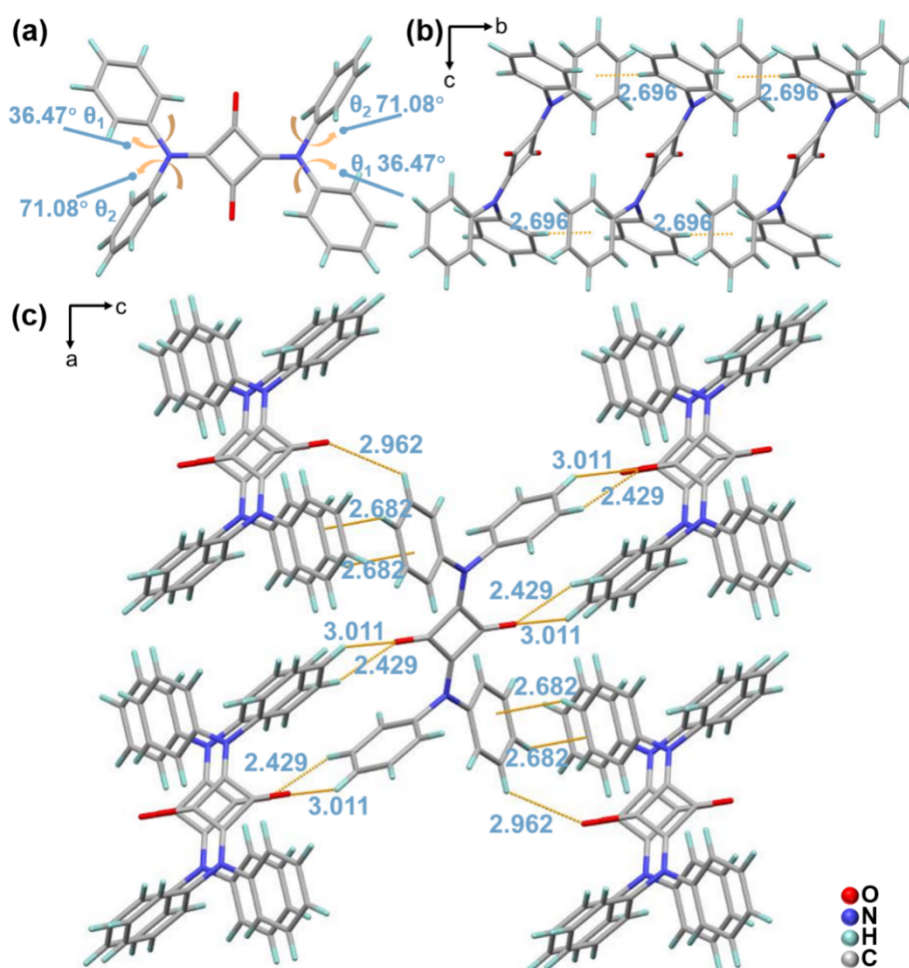
## Crystal data and crystal structure analyses of SQ-H and SQ-OMe

Table S4 Crystallographic data of SQ-H, SQ-OMe.

Sample	SQ-H	SQ-OMe
CCDC number	2239032	2239031
Empirical formula	C <sub>28</sub> H <sub>20</sub> N <sub>2</sub> O <sub>2</sub>	C <sub>32</sub> H <sub>28</sub> N <sub>2</sub> O <sub>6</sub>
Formula weight	416.46	536.56
<i>T</i> [K]	100(2)	100(2)
Crystal system	monoclinic	monoclinic
Space group	P 21/n	P 21/c
<i>a</i> [Å]	11.9476(2)	11.8624(4)
<i>b</i> [Å]	5.8409(10)	4.0641(2)
<i>c</i> [Å]	15.0139(3)	26.0523(9)
<i>α</i> [°]	90	90
<i>β</i> [°]	95.536(2)	94.013(3)
<i>γ</i> [°]	90	90
<i>V</i> [Å <sup>3</sup> ]	1042.85(3)	1252.90(9)
<i>Z</i>	2	2
F (000)	436	564
density [g/cm <sup>3</sup> ]	1.326	1.422
<i>μ</i> [mm <sup>-1</sup> ]	0.668	0.081
Reflections collected	9565	5898
unique reflections	2170	2601
<i>R</i> (int)	0.047	0.031
GOF	1.049	1.093
<i>R</i> <sub>I</sub> [ <i>I</i> > 2σ( <i>I</i> )]	0.040	0.045
<i>ωR</i> <sub>2</sub> [ <i>I</i> > 2σ( <i>I</i> )]	0.102	0.121
<i>R</i> <sub>I</sub> (all data)	0.043	0.052
<i>ωR</i> <sub>2</sub> (all data)	0.105	0.126



**Fig. S13** Fluorescence microscope images (under 365 nm UV illumination) of (a) SQ-H, (b) SQ-OMe crystals.



**Fig. S14** The molecular structure and packing mode in the SQ-H crystal. (a) The torsion angles between the four-membered ring and phenyl rotors in front view. Multiple intermolecular hydrogen-bonding and Ar-H $\cdots\pi$  interactions between adjacent SQ-H molecules along (b) b, c-axis and (c) a, c-axis.

SQ-H crystal belonged to a monoclinic crystal system and crystallized in the space group of P 21/n with two SQ-H molecules in one unit cell, taking the parameters of  $a = 11.9476$  (2),  $b = 5.84090$  (10) and  $c = 15.0139$  (3) Å. Notably, multiple intra/intermolecular hydrogen bonding served to construct the crystalline SQ-H, which essentially locked the phenyl rotations and subsequent ICT changes. As the natural propeller-like shape, the torsion angles between the four-membered ring and diphenylamine moieties were detected as  $\theta_1 = 36.47^\circ$  and  $\theta_2 = 71.08^\circ$  in SQ-H molecule (Fig. S14a). The molecular conformation was distorted, despite there existed several types of intermolecular Ar-H...O/ $\pi$  hydrogen bonding interactions. Along the b and c axis, there existed an Ar-H... $\pi$  interaction (2.696 Å) between adjacent SQ-H molecules (Fig. S14b). As shown in Fig. S14c, two types of moderate C=O...H hydrogen bonding (2.429 Å and 3.011 Å) between Ar-H and carbonyl in the central four-member ring were observed, which locked five molecules from two adjacent layers by the four-membered ring and one sloping side of phenyl rotors. Meanwhile, a C=O...H hydrogen bonding of 2.962 Å between Ar-H and carbonyl in the four-membered ring as well as two H... $\pi$  interactions (2.682 Å) between the other side of phenyl rotors from adjacent five molecules in two layers were also observed along the a and c axis. As such, this special packing mode, dominated by multiple intermolecular C-H...O and C-H... $\pi$  interactions, would well support the fact that SQ-H exhibited no piezochromic behavior.



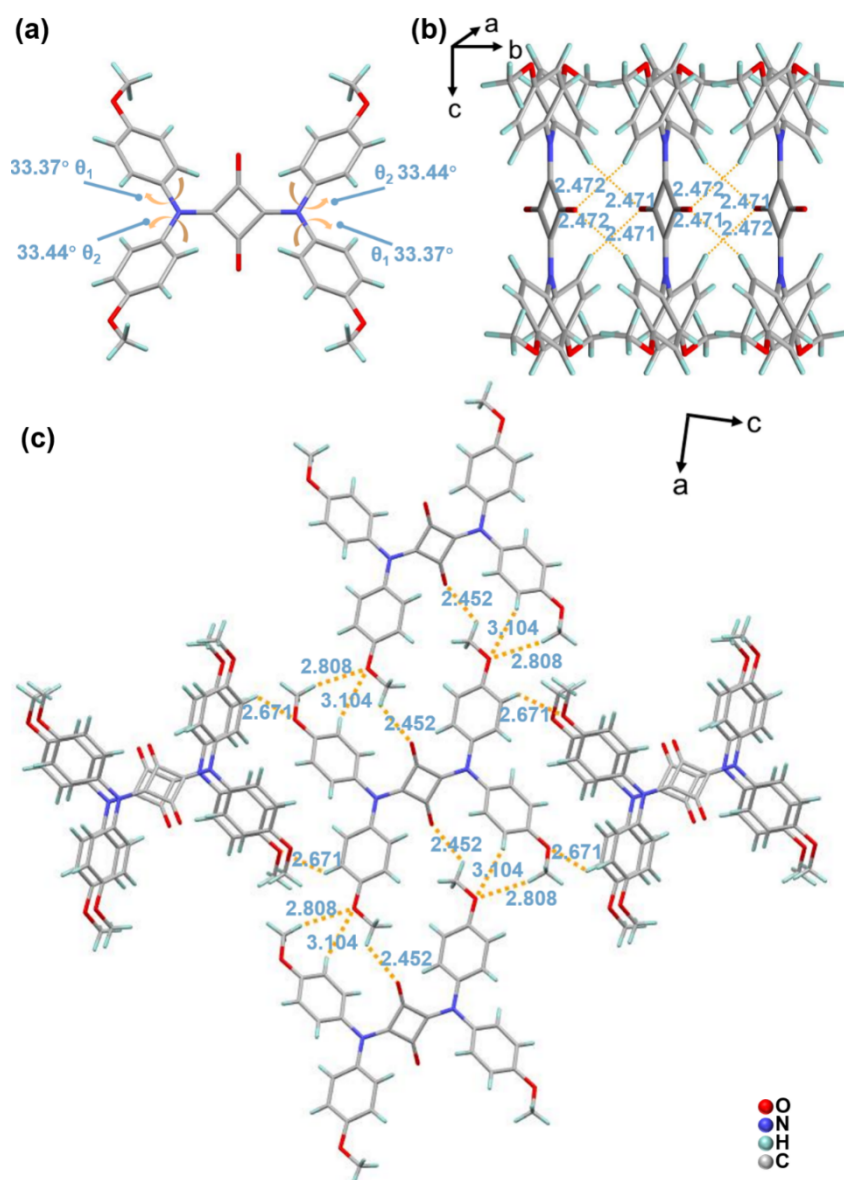


**Fig. S15** The molecular structure and packing mode in the SQ-OMe crystal. (a) The torsion angles between the four-membered ring and phenyl rotors in front view. Multiple intermolecular hydrogen-bonding interactions between adjacent SQ-OMe molecules along (b) b, c-axis and (c) a, c-axis.

SQ-OMe crystal belonged to a monoclinic crystal system and crystallized in the space group of P 2<sub>1</sub>/c with two SQ-OMe molecules in one unit cell taking the parameters of  $a = 11.8624(4)$ ,  $b = 4.0641(2)$  and  $c = 26.0523(9)$  Å. Due to the strong intermolecular interactions in interior of every layer, the whole SQ-OMe is more planar than SQ-H. The torsion angles between the four-membered ring and phenyl moieties were detected as  $\theta_1 = 33.37^\circ$  and  $\theta_2 = 33.44^\circ$  in it (Fig. S15a). As shown in Fig. S15b,

two types of strong Ar-H...O hydrogen bonding interactions (2.471 Å and 2.472 Å) were observed between adjacent two SQ-OMe molecules in one cluster, which was mutual deadlock with each other between Ar-H and carbonyl in the four-membered ring. It contributes to locking the phenyl rotors. In Fig. S15c, there are also two types of Ar-H...O hydrogen bonding interactions (2.671 Å and 3.104 Å) that can lock phenyl rotations. Furthermore, two types of C-H...O hydrogen bonding interactions (2.452 Å and 2.808 Å) between adjacent SQ-OMe molecules can also be observed along the a and c axis. The multiple moderate to strong Ar-H...O interactions locking the phenyl rotations enhanced intramolecular rigidity of SQ-OMe, which results in no piezochromic behavior.

## **Characterizations and all photophysical data of SQ-H and SQ-OMe microcrystals**

The maximum peaks of PL spectra in the crystal of SQ-H and SQ-OMe were 533 nm and 592 nm (Fig. S16). It is obvious that there is a wide-range red shift in the aggregation state, which demonstrates the significance of conformational planarization to luminescence behavior. The simulated XRD patterns of SQ-H and SQ-OMe crystals turned out to be consistent with that of their crystalline assemblies (Fig. S17), suggesting the same molecular packing modes. In common organic solvents, the UV-vis spectra of SQ-H and SQ-OMe were recorded with maximum absorption peaks centered at 410 nm and 420 nm (Fig. S18). Similar to SQ-NMe<sub>2</sub>, no fluorescence emission was observed. In DMF / water mixtures, SQ-H and SQ-OMe also displayed gradual red-shift in PL spectra with increasing the water fractions, and they exhibited structureless fluorescence emissions with maximum peak ( $\lambda_{em}$ ) at 503 nm and 566 nm upon forming aggregates, suggesting typical AIE phenomenon (Fig. S19-20).<sup>1,2</sup> TGA experiments revealed that SQ-H and SQ-OMe microstructures were stable until 356.77 °C and 382.55 °C (Fig. S21). The lifetime decay profiles of SQ-H and SQ-OMe were tested by a single-photocounting method with a longer lifetime than SQ-NMe<sub>2</sub> of 2.60

ns and 4.11 ns (Fig. S22), which matched well with the molecular interaction between luminophores.<sup>3</sup>

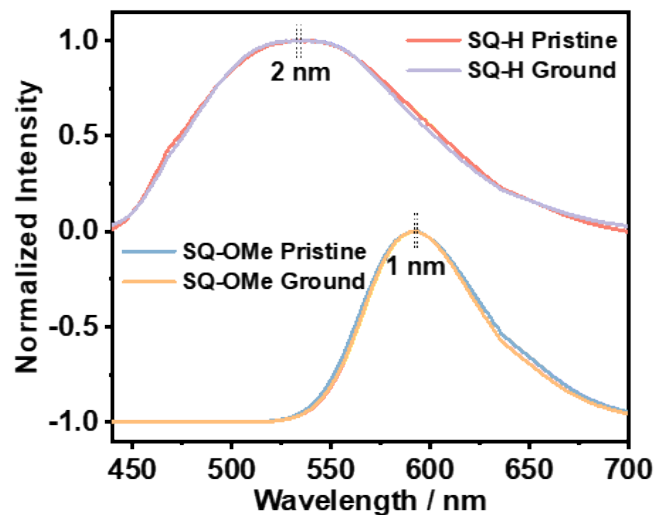


**Fig. S16** Normalized PL spectra of SQ-H and SQ-OMe in pristine and ground states.

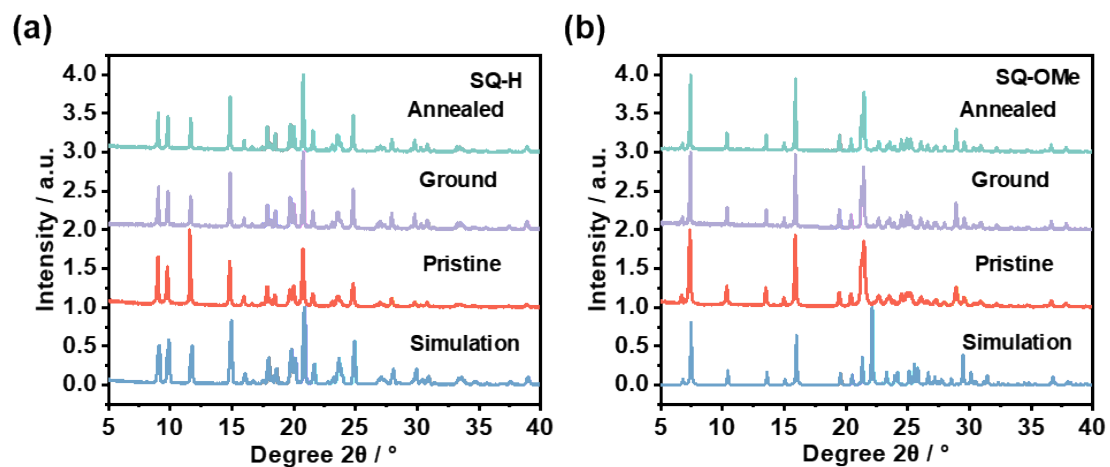


**Fig. S17** PXRD patterns of (a) SQ-H, (b) SQ-OMe in simulated, pristine, ground and annealed (140 °C for 1 min) states.

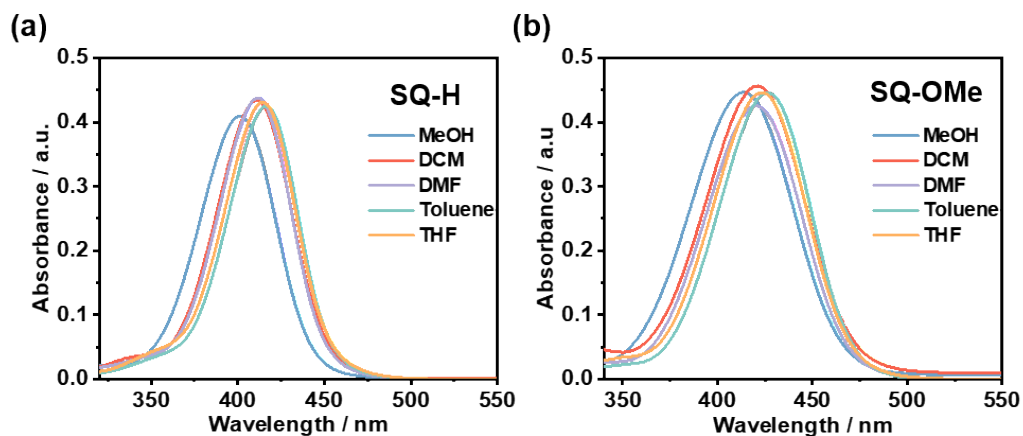


**Fig. S18** Absorption spectra of SQ-H, SQ-OMe (50  $\mu$ M) in different solvents.

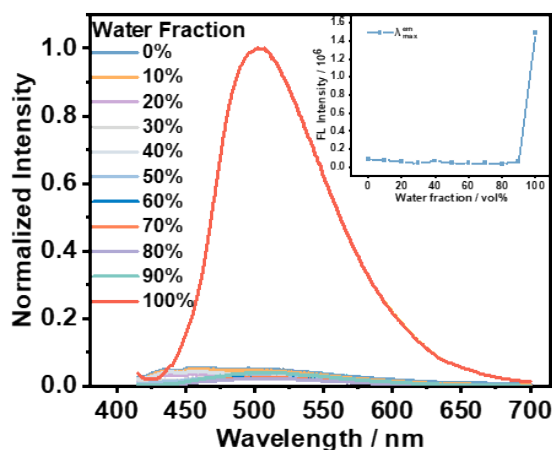


**Fig. S19** PL spectra of SQ-H (50  $\mu$ M) in DMF solution with different fractions of water. (Inset: Plots of  $\lambda_{em\ max}$  with different fractions of water, where  $\lambda_{em\ max}$  depict the maximum emission intensity.)

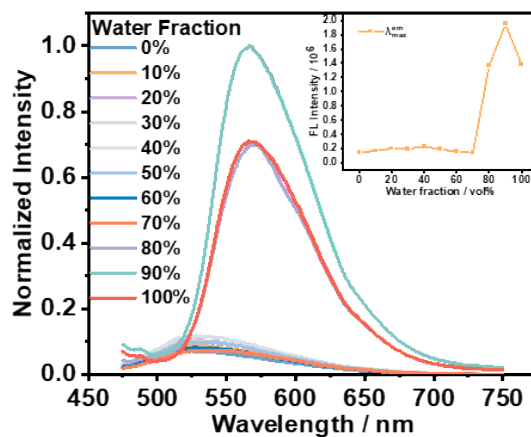


**Fig. S20** PL spectra of SQ-OMe (50  $\mu$ M) in DMF solution with different fractions of water. (Inset: Plots of  $\lambda_{em\ max}$  with different fractions of water, where  $\lambda_{em\ max}$  depict the maximum emission intensity.)

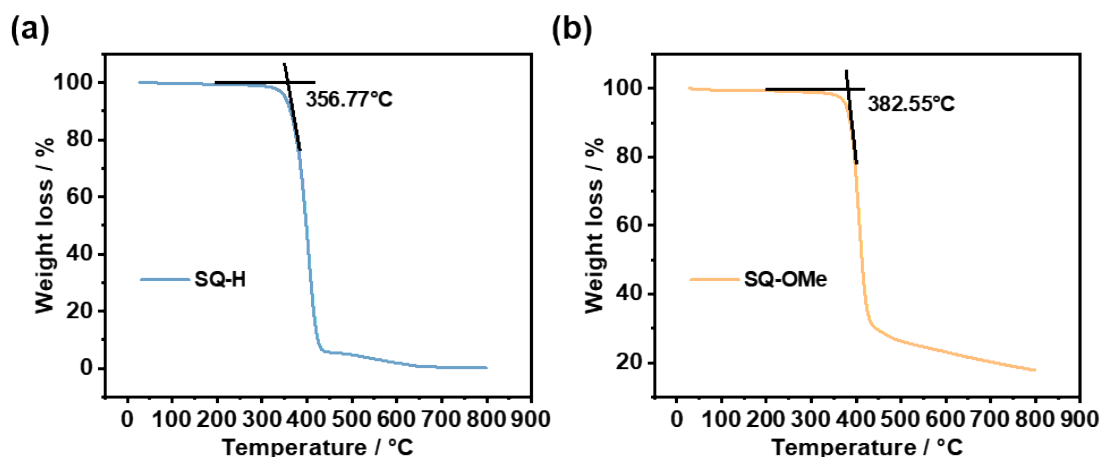


**Fig. S21** TGA curves of (a) SQ-H, (b) SQ-OMe microcrystals. The scanning rate is 20 °C min<sup>-1</sup> under N<sub>2</sub>.

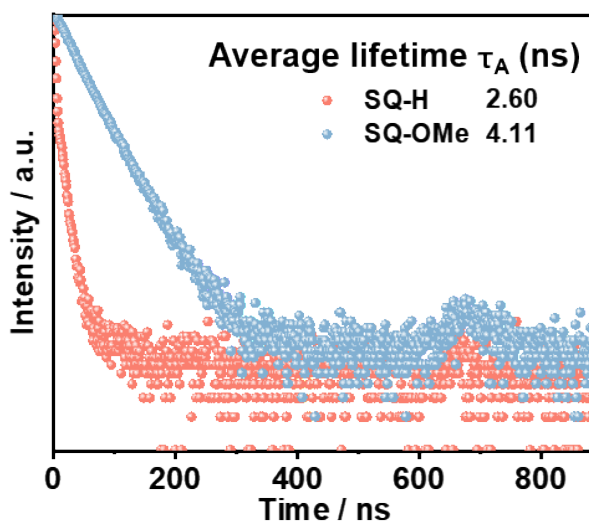


**Fig. S22** Lifetime decay profiles of SQ-H and SQ-OMe in crystal.

**Table S5** The photophysical data for SQ-H, SQ-OMe in crystal at 298 K.

Microcrystals	$\lambda_{em}$ <sup>a)</sup> [nm]	$\Phi_{PL}$ <sup>b)</sup> %	Lifetime $\tau_f$ <sup>c)</sup> [ns]	$\chi^2$	$k_f$ <sup>d)</sup> [10 <sup>7</sup> s <sup>-1</sup> ]	$k_{nr}$ <sup>e)</sup> [10 <sup>7</sup> s <sup>-1</sup> ]
SQ-H	517	42.0	2.60	1.07	16.15	22.31
SQ-OMe	589	59.4	4.11	1.09	14.45	9.88

<sup>a)</sup> Measured using an integrating sphere method; <sup>b)</sup> Measured using a single-photon counting method; <sup>c)</sup> Radiative rate constant ( $k_f = \Phi_{PL} / \tau_f$ ); <sup>d)</sup> Nonradiative rate constant ( $k_{nr} = (1 - \Phi_{PL}) / \tau_f$ ).

## Computational study

**Computational methods:** For the DFT calculations, all the computations were done within the Gaussian 09<sup>4</sup> program at the B3lyp/6-311g(d) level. The absorption spectra and oscillator strength of SQ-H, SQ-OMe, and SQ-NMe<sub>2</sub> were calculated by time-dependent density functional theory (TD-DFT). Emission spectra of SQ-NMe<sub>2</sub> at different torsion angles were calculated by TD-DFT, too. One side of the torsion angle between the four-membered ring and phenyl rotor was frozen at 30°, together with the other side at 80°, 65°, 43°, and 30°, respectively. The two models of torsion angles at 65° and 43° correspond to single crystal SQ-NMe<sub>2</sub> Y-form and O-form, respectively.

**Table S6** Summary of the oscillator strengths of SQ-H, SQ-OMe and SQ-NMe<sub>2</sub> in gas state calculated using B3LYP/6-31G(d) by Gaussian 09.

	Calculation (nm)	Electronic transition	oscillator strength (f)	E <sub>Vert</sub>	Experiment (nm)
SQ-H	404	HOMO→LUMO (99.3%)	0.7635	S <sub>0</sub> →S <sub>1</sub>	411
SQ- OMe	413	HOMO→LUMO (99.3%)	0.8644	S <sub>0</sub> →S <sub>1</sub>	420
SQ- NMe <sub>2</sub>	439	HOMO→LUMO (99.2%)	0.9709	S <sub>0</sub> →S <sub>1</sub>	459

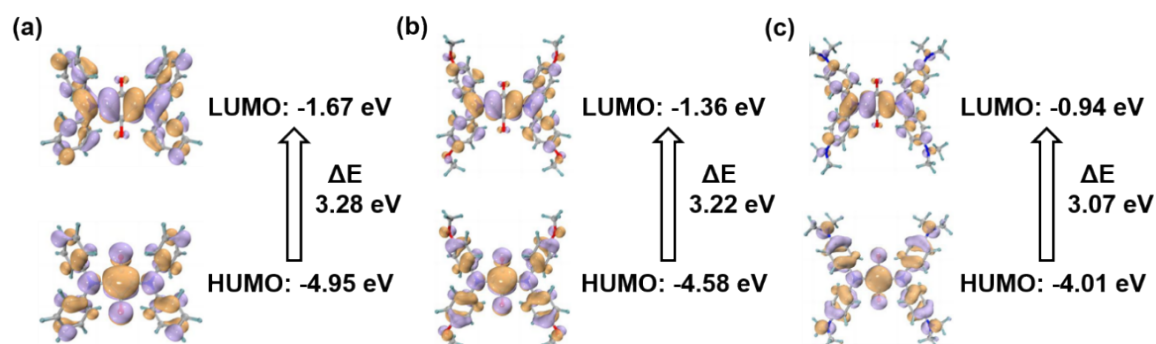


**Fig. S23** The theoretical calculated ground-state frontier orbitals contribution of (a) SQ-H, (b) SQ-OMe and (c) SQ-NMe<sub>2</sub> in gas state using B3LYP/6-31G(d) by Gaussian 09.

## Details of cryptographic application

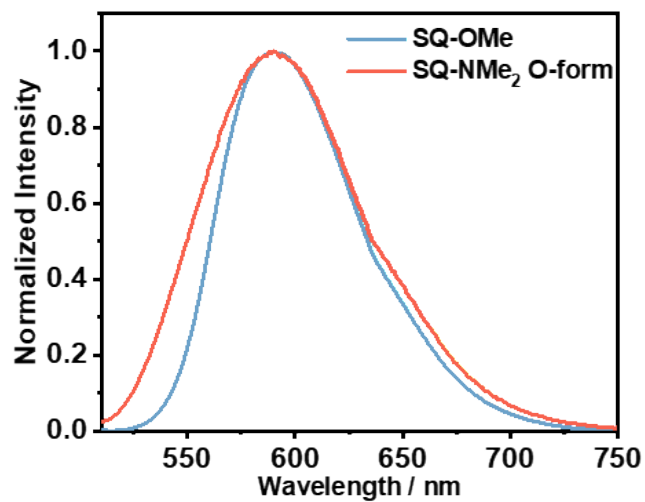


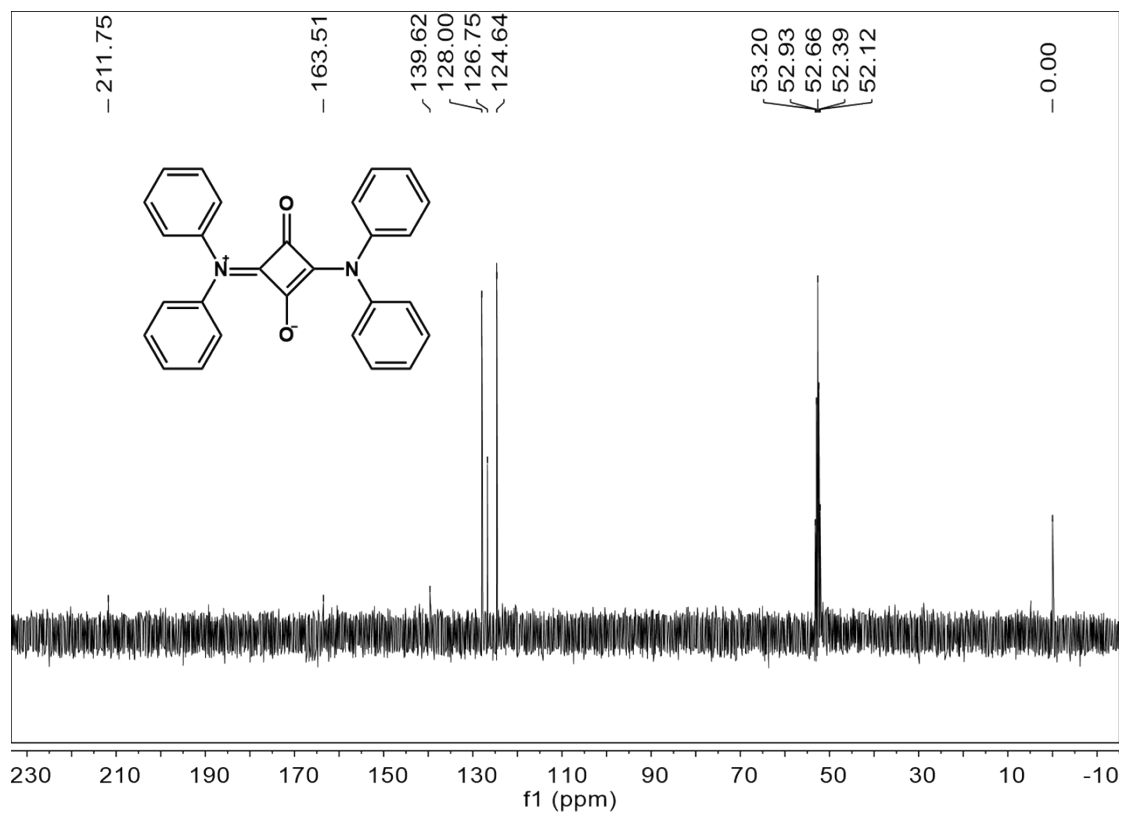
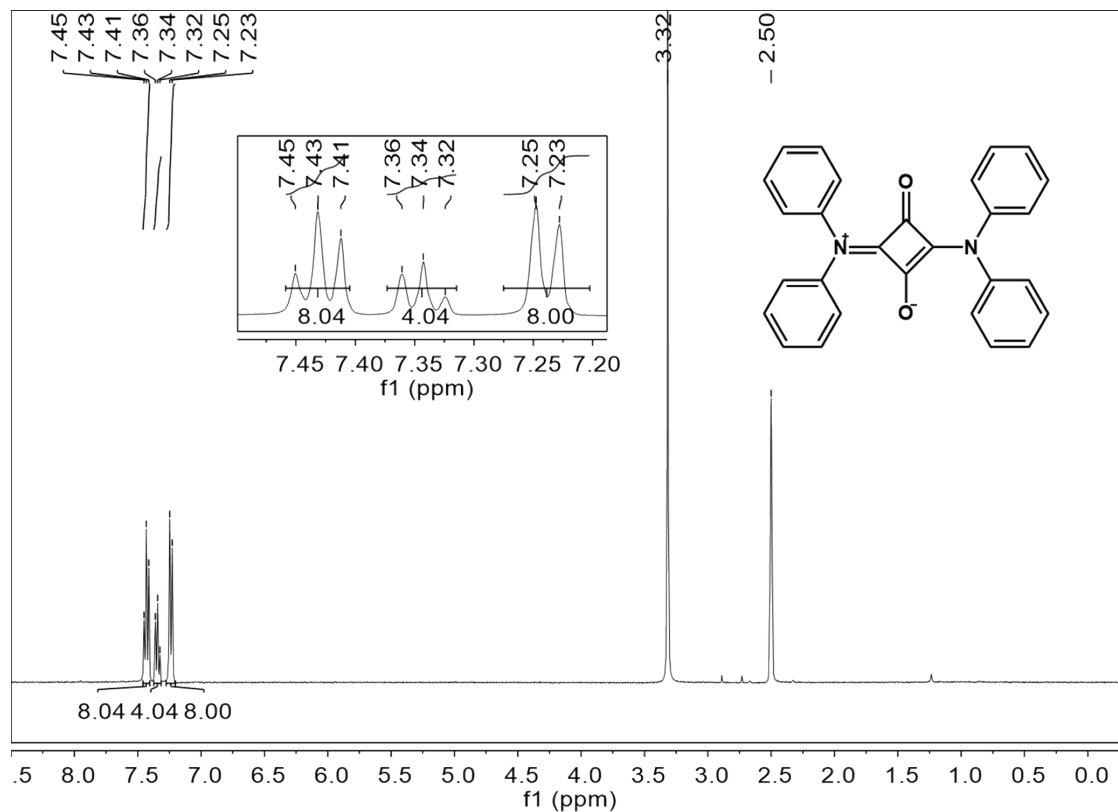
**Fig. S24** Normalized PL spectra of SQ-OMe and SQ-NMe<sub>2</sub> O-form which were used in the QR code.

### Morse Code

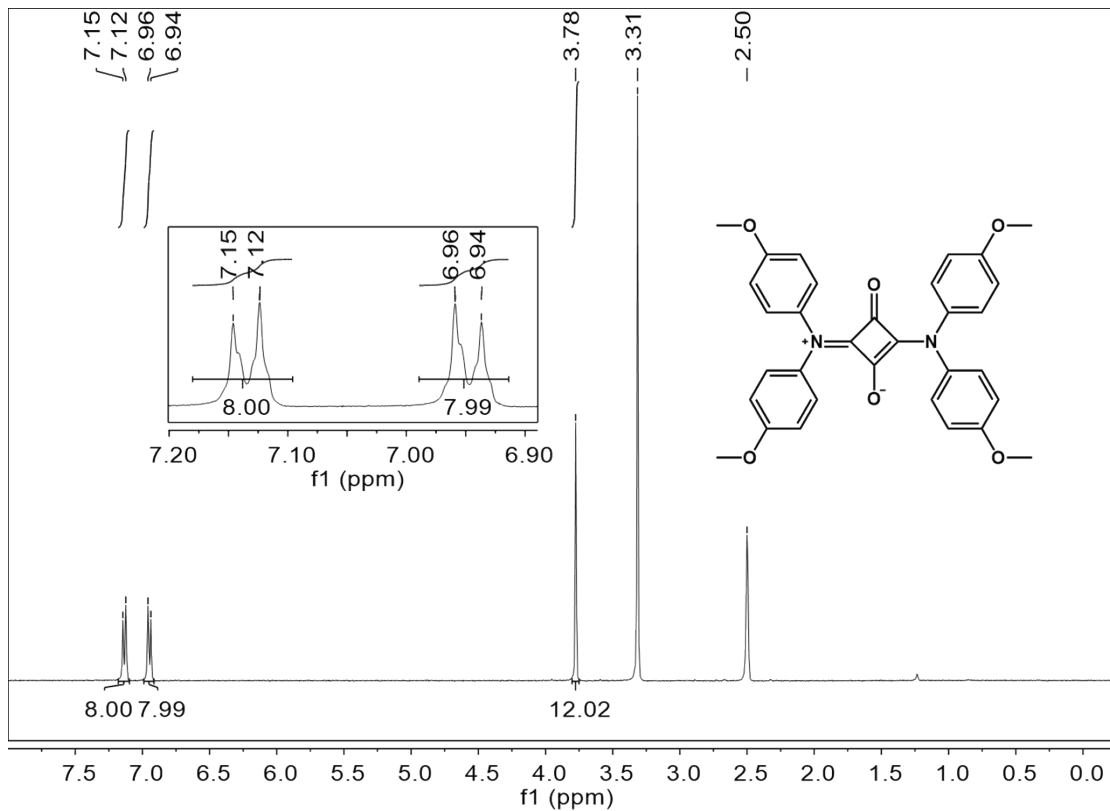
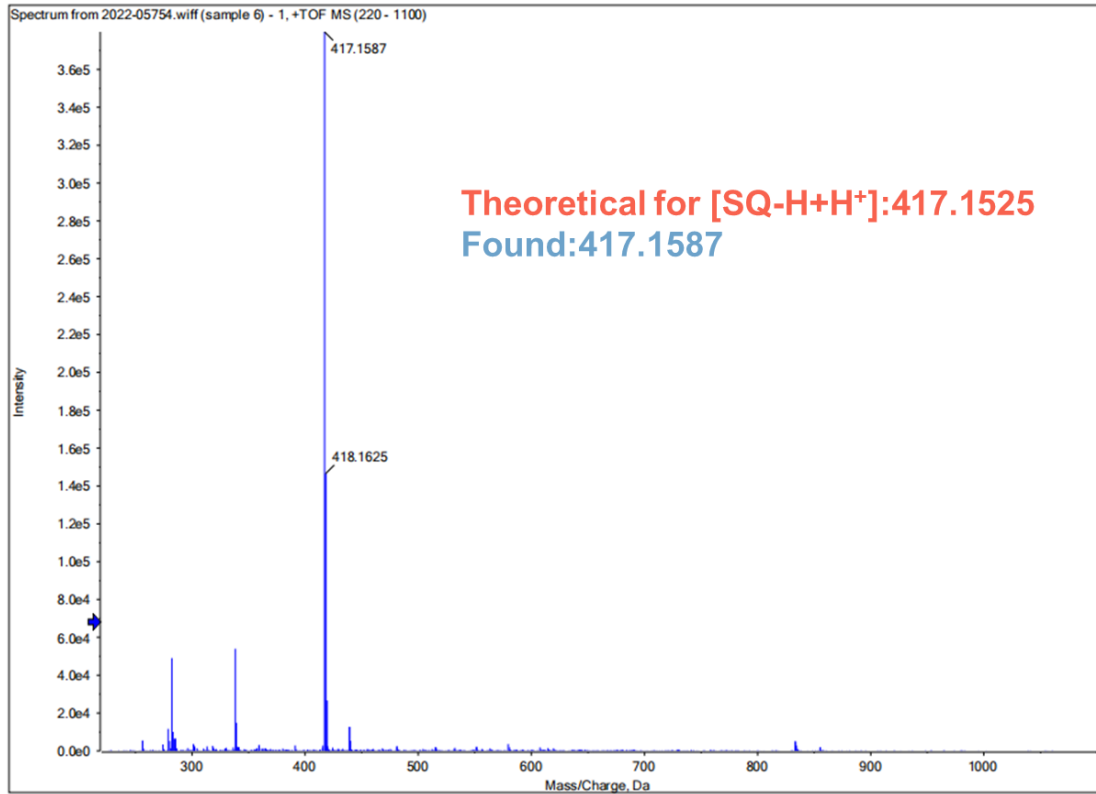
A	• —	M	— —
B	— •••	N	— •
C	— • — •	O	— — —
D	— ••	P	• — — •
E	•	Q	— — • —
F	•• — •	R	• — •
G	— — •	S	•••
H	••••	T	—
I	••	U	•• —
J	• — — —	V	••• —
K	— • —	W	• — —
L	• — ••	X	— •• —

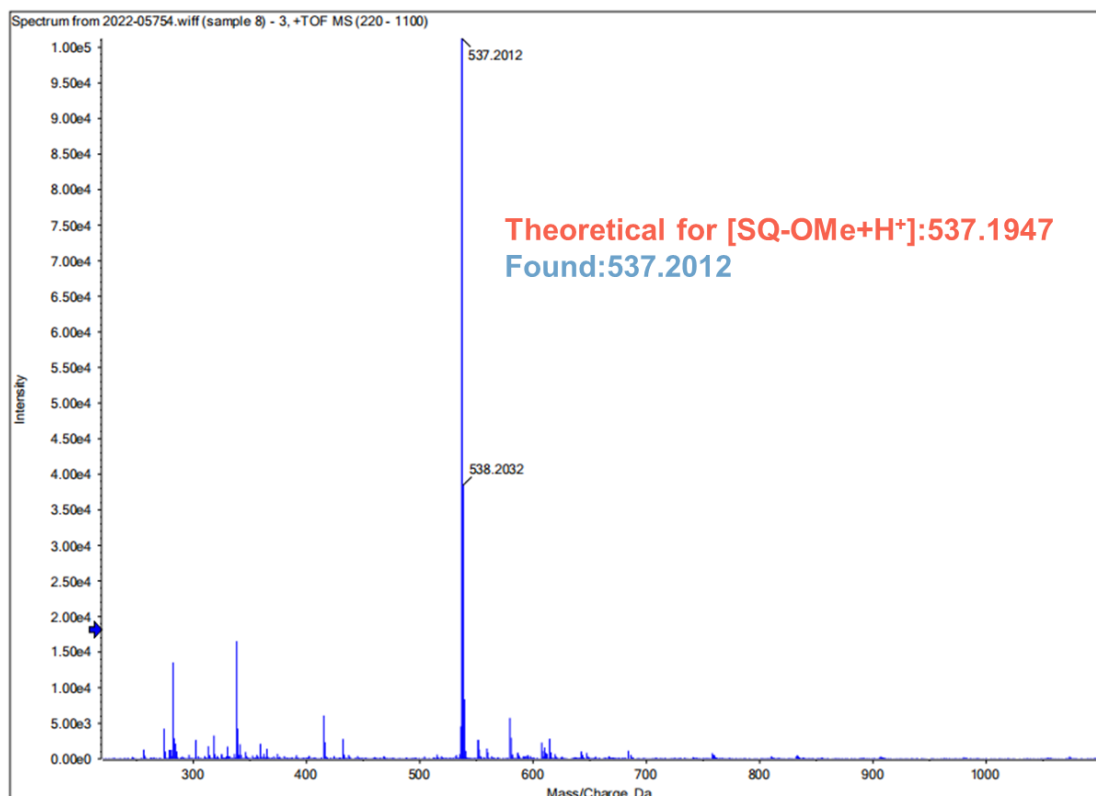
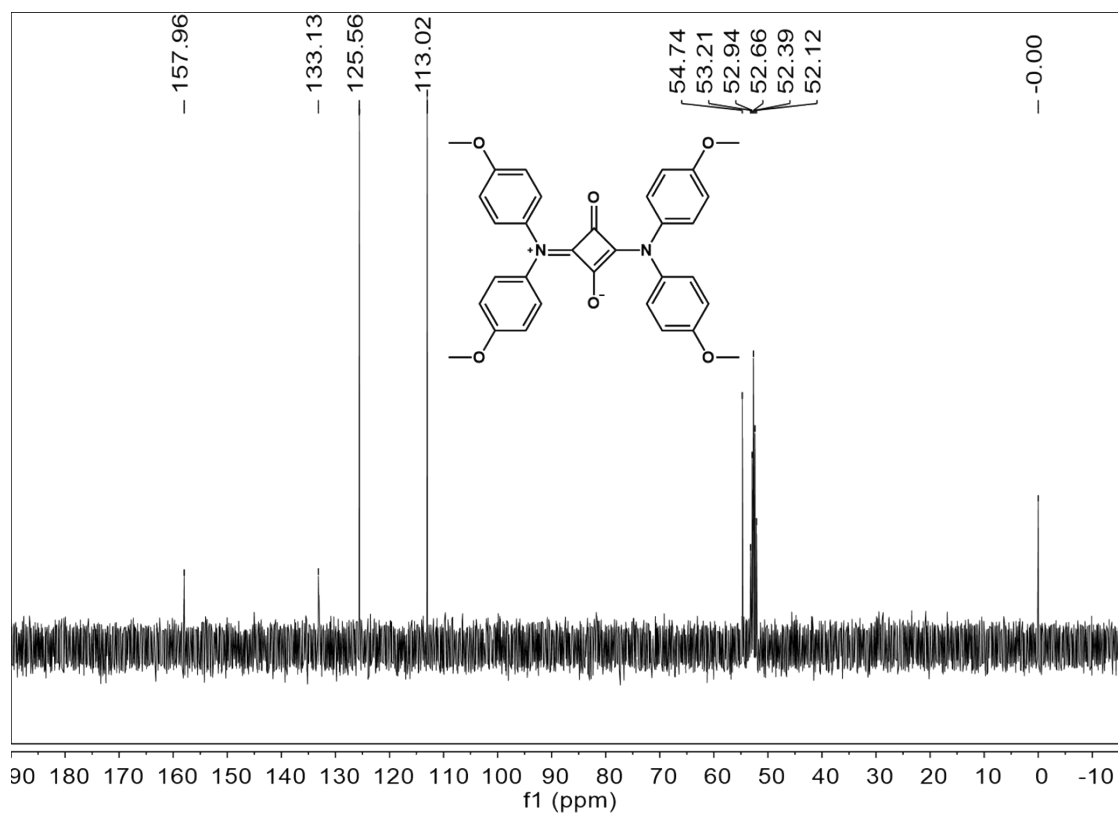
**Fig. S25** International Morse code for translation.

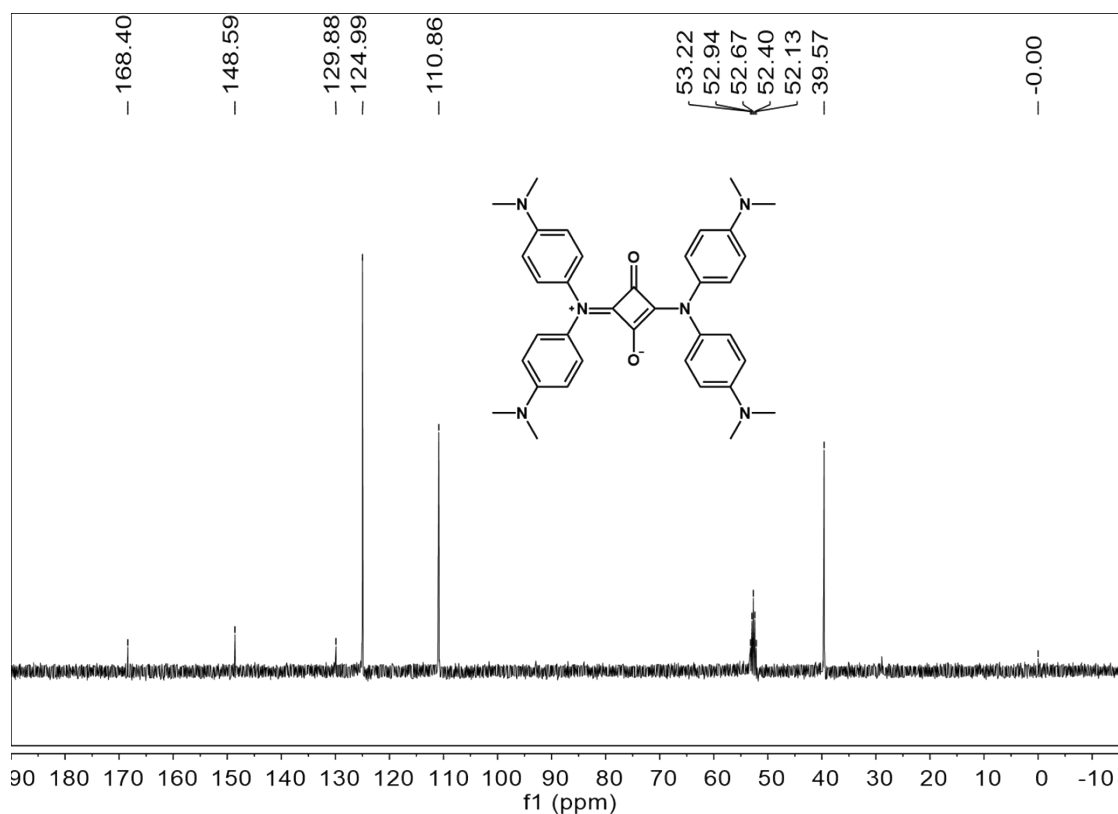
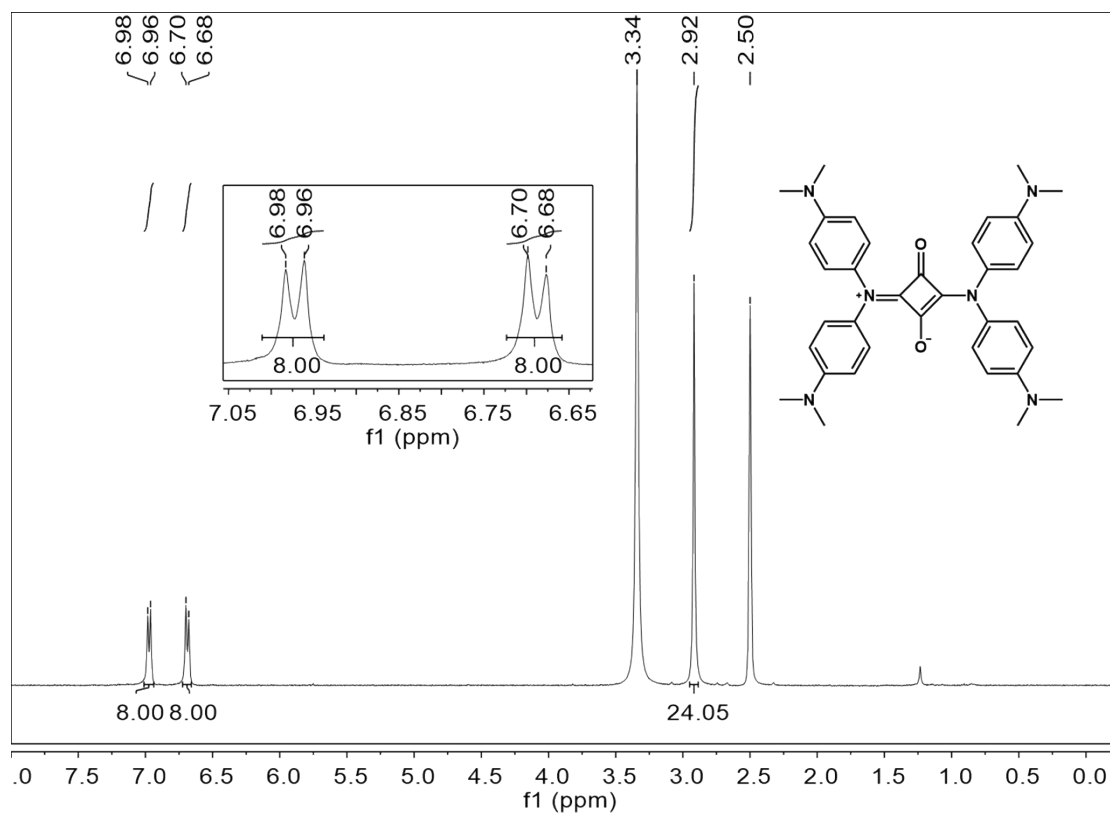
# $^1\text{H}$ NMR, $^{13}\text{C}$ NMR and MS spectra

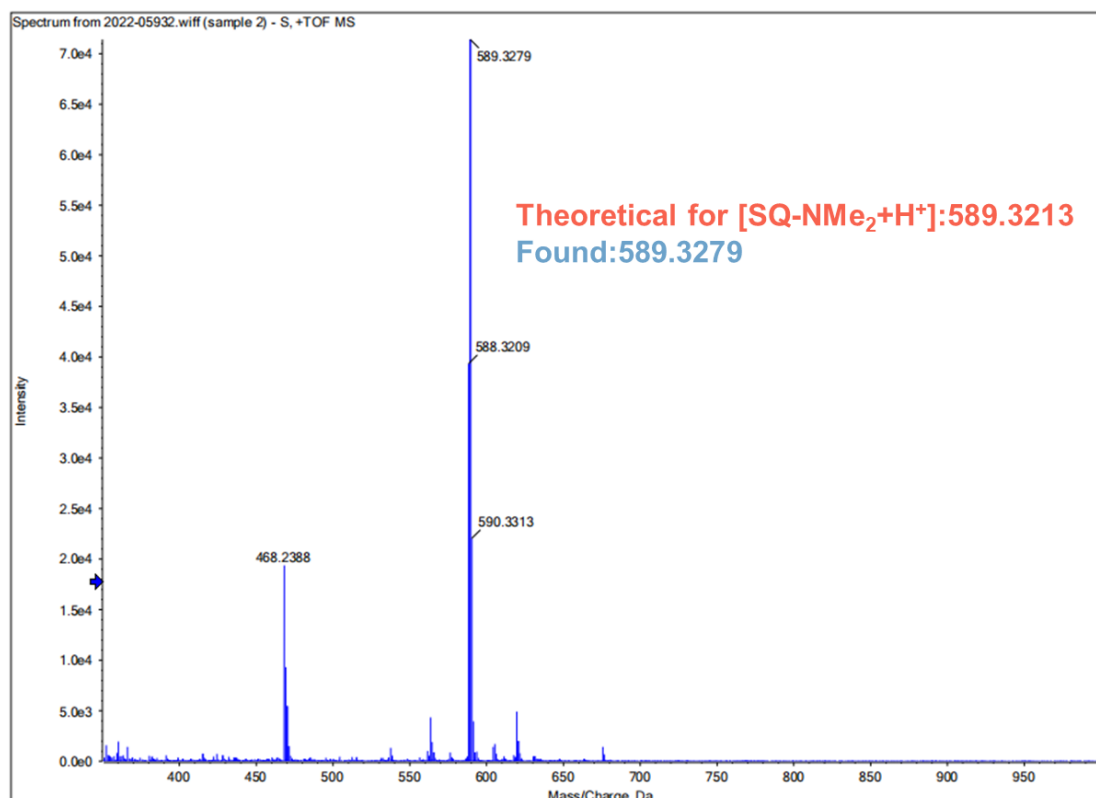












## References

- 1 Y. Q. Dong, J. W. Lam and B. Z. Tang, *J. Phys. Chem. Lett.*, 2015, 6, 3429-3436.
- 2 P.-Z. Chen, H. Zhang, L.-Y. Niu, Y. Zhang, Y.-Z. Chen, H.-B. Fu and Q.-Z. Yang, *Adv. Funct. Mater.*, 2017, 27, 1700332.
- 3 X. Zhu, S. W. Dai, Y. L. Lai, Y. Dou, M. Wang, J. S. Ho, Y. A. Chang, Y. T. Chuang, H. W. Lin and B. Hu, *J. Phys. Chem. Lett.*, 2021, 12, 11894-11901.
- 4 M. J. Frisch, G. W. Trucks, H. B. Schlegel, G. E. Scuseria, M. A. Robb, J. R. Cheeseman, G. Scalmani, V. Barone, B. Mennucci, G. A. Petersson, H. Nakatsuji, M. Caricato, X. Li, H. P. Hratchian, A. F. Izmaylov, J. Bloino, G. Zheng, J. L. Sonnenberg, M. Hada, M. Ehara, K. Toyota, R. Fukuda, J. Hasegawa, M. Ishida, T. Nakajima, Y. Honda, O. Kitao, H. Nakai, T. Vreven, J. A. Montgomery Jr, J. E. Peralta, F. Ogliaro, M. Bearpark, J. J. Heyd, E. Brothers, K. N. Kudin, V. N. Staroverov, R. Kobayashi, J. Normand, K. Raghavachari, A. Rendell, J. C. Burant, S. S. Iyengar, J. Tomasi, M. Cossi, N. Rega, J. M. Millam, M. Klene, J. E. Knox, J. B. Cross, V. Bakken, C. Adamo, J. Jaramillo, R. Gomperts, R. E. Stratmann, O. Yazyev, A. J. Austin, R. Cammi, C. Pomelli, J. W. Ochterski, R. L. Martin, K. Morokuma, V. G. Zakrzewski, G. A. Voth, P. Salvador, J. J. Dannenberg, S. Dapprich, A. D. Daniels, O. Farkas, J. B. Foresman, J. V. Ortiz, J. Cioslowski, D. J. Fox, Gaussian 09 (Revision A.02), Gaussian Inc., Wallingford CT, 2009.